Received: 2 October 2024 | Accepted: 25 March 2025

DOI: 10.1111/afe.12686

ORIGINAL ARTICLE

Agricultural and Forest Entomology

Stabilizing adaptation in an invasive species: Alfalfa weevil as a case study

Andrew Paul Gutierrez[1,2] | Luigi Ponti[1,3] | Alexandre Levi-Mourao[4] | Xavier Pons[4] | José Ricardo Cure[1,5] | Markus Neteler[1,6] | George Simmons[7]

[1]Center for the Analysis of Sustainable Agricultural Systems (www.casasglobal.org), Kensington, California, USA

[2]Division of Ecosystem Science, College of Natural Resources, University of California, Berkeley, California, USA

[3]Agenzia nazionale per le nuove tecnologie, l'energia e lo sviluppo economico sostenibile (ENEA), Centro Ricerche Casaccia, Rome, Italy

[4]Department of Crop Protection and Forest Sciences, University of Lleida, Lleida, Spain

[5]Facultad de Ciencias Básicas y Aplicadas, Universidad Militar Nueva Granada, Bogotá, Colombia

[6]Mundialis GmbH & Co. KG, Bonn, Germany

[7]IDEMS International, Berkshire, UK

Correspondence
Andrew Paul Gutierrez, Center for the Analysis of Sustainable Agricultural Systems, Kensington, CA 94707-1035, USA.
Email: casas.global@berkeley.edu

Luigi Ponti, Agenzia nazionale per le nuove tecnologie, l'energia e lo sviluppo economico sostenibile (ENEA), Centro Ricerche Casaccia, Rome, Italy.
Email: luigi.ponti@enea.it

Funding information
Ministero dell'Università e della Ricerca, Grant/Award Number: ARS01_00815; McKnight Foundation, Grant/Award Numbers: 22-341, 24-124; Ministerio de Ciencia, Innovación y Universidades, Grant/Award Number: AGL2017-84127-R

Abstract

1. Studies on the phylogeographic structure of species (strains) have yielded insights into their geographic distribution but tell less about strain's capacity to invade novel environments.
2. Extensive age-specific life table data on two strains of the invasive Palearctic alfalfa weevil, *Hypera postica* (Gyllenhal) (i.e., Ebro Valley, Spain (*S*) and Hamadan, Iran (*I*) strains) having disparate vital rates, are used to develop weather-driven physiologically based demographic models (PBDMs) of their biology. The PBDMs are used to explore prospectively their invasive potential across much of the Holarctic.
3. Using N.E. Gilbert's theory that fecundity is selected to the level appropriate for the population in its environment, we explore the interacting effects of multiples of observed fecundity, temperature-dependent mortality and density-dependent population growth constraints on stabilizing adaptation in strains *S* and *I* to weather in their native area. Aestivating adults (^{aes}A) bridge the critical winter period, and their annual production is used as a metric of adaptation. Maximization of ^{aes}A in the native environments supports Gilbert's supposition.
4. The *S* and *I* strains have wide invasive potential, and we posit stabilizing selection for maximizing ^{aes}A would occur after successful invasion of novel environments.
5. We propose that the evolving adaptation of an invasive strain to extant and climate change weather can be examined by periodic updates of the biodemographic biology in the weather-driven PBDMs.

KEYWORDS
geographic distribution, invasive species, pest risk analysis, physiologically based demographic models, population dynamics, relative abundance, stabilizing selection, strains

INTRODUCTION

Research on adaptation of invasive species to novel environments (e.g., Le Roux, 2021; Moran & Alexander, 2014) and their phylogeographic structure (e.g., Biedrzycka et al., 2022; Du et al., 2023; Hadjistylli et al., 2016) has yielded limited generality on their invasiveness as measured by potential geographic distribution and relative abundance. Species with wide geographic distributions may exhibit phylogeographic structure, with lineages (strains) adapted to local biotic and abiotic conditions. A strain is defined as a population of

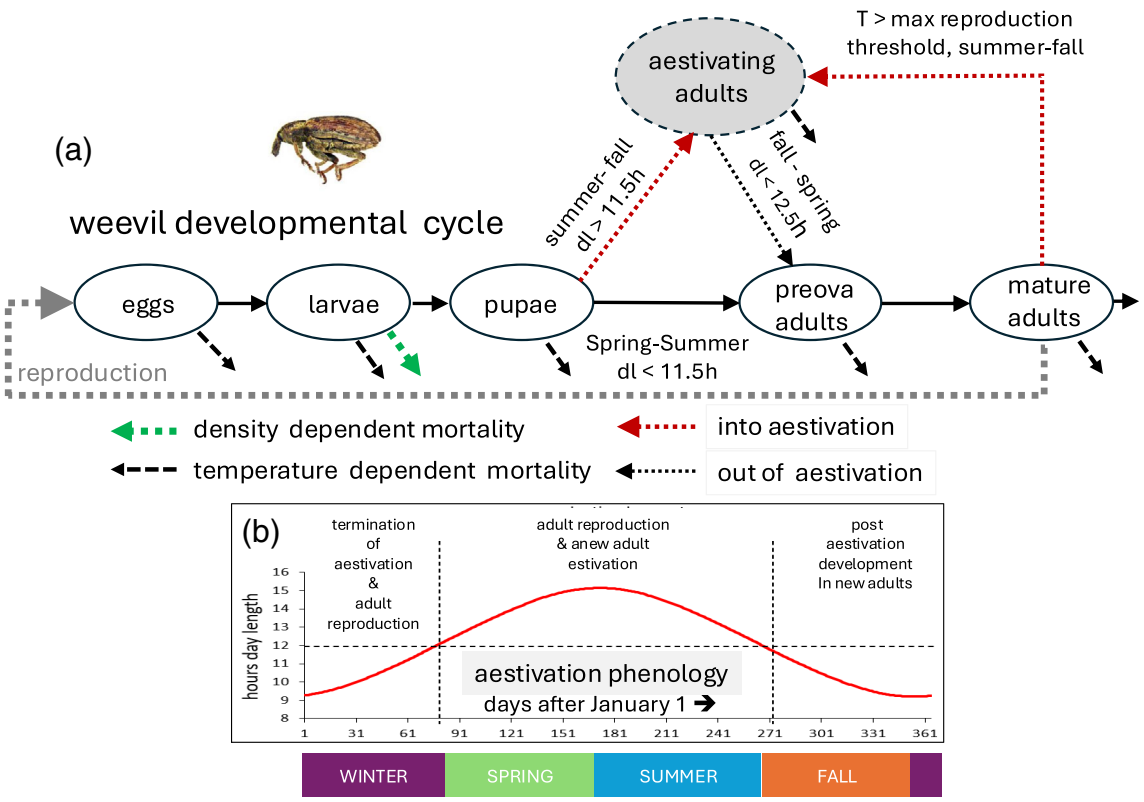

FIGURE 1 Developmental biology of the alfalfa weevil: (a) egg, larval and pupal, and preoviposition, reproductive and aestivating adult stages, and (b) the reproductive states of adult weevils in response to hours (h) day length. The red dotted arrows in 1a indicate entry into aestivation of new adults and of reproductive adults, and the dark dotted arrow indicates termination of aestivation during the fall to early spring period. Some new adults may not enter aestivation and produce a second generation, temperature-dependent mortality occurs in all stages (dashed black arrows) and density-dependent mortality occurs in the larval stage (green dashed arrow).

individuals of the same species having similar vital rates adapted to conditions in a geographic region (c.f., Downie, 2010). An invasive strain may invade a novel area from any part of its range (see Godefroid et al., 2015; Messenger & van den Bosch, 1969) with its behavioural and physiological traits determining establishment success (DeBach, 1964). Further, its natural enemies may co-evolve (e.g., Salt & van den Bosch, 1967) making discovery of adapted natural enemies for biological control challenging.

Alfalfa (*Medicago sativa* L.) was likely domesticated in modern-day Iran and Türkiye (Brough et al., 1977) and spread globally as a major forage crop (Tang et al., 2024). The alfalfa weevil, *Hypera postica* (Gyllenhal), co-occurs with alfalfa over its vast Palearctic range and, as an invasive species, has become a major pest of alfalfa across the Holarctic. Several strains of alfalfa weevil have been documented (e.g., Coles & Day, 1977; Sanaei & Seiedy, 2016; Schroder & Steinhauer, 1976; Tuda et al., 2021), and the weevil invaded North America from unknown areas of its Palearctic range at least three times. The 'western' strain entered the Salt Lake Valley of Utah in 1904 (Titus, 1910), the 'Egyptian' strain was found in Yuma, Arizona, in 1939 (Wehrle, 1940) and the 'eastern' strain in Maryland in 1952 (Poos & Bissell, 1953). The eastern strain is distributed across the central and eastern regions of the United States, the western strain is distributed in central California and across the northwestern United States, and the Egyptian strain is found in the southwestern United States (Böttger et al., 2013), but areas of intergrade occur (see Bundy et al., 2005). Sanaei et al. (2016) sequenced the mitochondrial COI gene of populations from Iran, Poland and the Czech Republic and detected two groups that suggest the European populations may be the western US strain, with the western and Egyptian/eastern strains co-occurring in Iran. Tuda et al. (2021) made a comprehensive analysis of the spatial genetic structure of the weevil in the Palearctic, and though behavioural, taxonomic and genomic studies can detect differences, they are insufficient to assess strain invasiveness; this requires biodemographic data on their biology sufficient to model their weather-driven population dynamics in the invaded area.

A general physiologically based demographic model (PBDM, see Appendix) for the supposedly Egyptian strain (designated *E*) (Gutierrez et al., 1976) was developed as a component of a larger modular alfalfa system model composed of 14 interacting species (see Gutierrez & Ponti, 2013). This heritage model for the *E* strain was based on laboratory data for a population from the desert regions of Arizona and California (Butler & Ritchie, 1967; Gutierrez et al., 1976). The general biology of all known alfalfa weevil strains is similar (Figure 1); hence, the *E* strain model was easily recast in a modular structure to include the biology for strains from the Ebro Valley, Spain and Hamadan, Iran, hereafter designated the *S* (Spain) and *I* (Iran) strains. Additional

TABLE 1 Stage-specific parameters and developmental times.

Stage	θ_L[a]	θ_U[b]	$dd > \theta_L$
Ebro Valley, Spain (*S* strain; Levi-Mourao et al., 2021, 2022)			
Egg	6.85	37.5	118.3
Larval stages	6.25	36. 5	270.4
Pupa	6.75	36.85	74.1
Pre-viposition period	5.5	27.5	487.8
Adult longevity (mean)	5.5	27.5	1015.0
Hamadan, Iran (*I* strain; Zahiri et al., 2010a, 2010b)			
Egg	10.75	35.5	100.7
Larval stages	10.75	35.5	164.36
Pupa	10.75	35.75	108.36
Preoviposition period	4.37	33.5	643.86
Adult longevity (mean)	4.37	33.5	∼2071
Arizona—Southern California (*E* strain; Butler Jr. & Ritchie Jr., 1967; Gutierrez et al., 1976)[c]			
Egg	7.2	33	117.2
Larval stages	7.2	33	207.0
Pupa	7.2	33	157.0
Preoviposition period	7.2	33.5	155.0
Adult longevity (mean)	7.2	33.5	∼1150

Note: Sources of the parameter estimates are indicated in the table.
[a]θ_L is the low temperature when the rate of development is zero.
[b]θ_U is the upper temperature where the developmental rate begins to decline to zero.
[c]Parameters from Gutierrez et al., 1976.

strains can easily be incorporated in the computer algorithm coded in Borland Pascal, and any of the strains can be included in a simulation run using a Boolean variable. The *S* and *I* strains are the major focus of our study to explore prospectively their invasive potential across the Euro-Palearctic region and the United States, Mexico and Central America and to explore adaptation of strains *S* and *I* to weather in their native Palearctic environments.

As background, the Ebro Valley (41° 37′ N, 00° 38′ E, elevation 155 m) has a temperate semi-arid climate (Köppen *BSk*) (Baranowski et al., 2015) with mild winters and dry moderate summers with maximum temperatures occasionally exceeding 30°C. Frosts are common during winter with occasional snowfall, and average precipitation of 369 mm per year with peaks in April–May and in September–October. Hamadan, Iran (34°58′ N, 48°26′ E; elevation, 1710 m) has long cold winters with extreme low temperatures and high maximum summer temperatures (Aḏkā'i, 2003). The desert regions of Arizona and California (e.g., Brawley, Ca., 32° 44′ N, 114° 57′ W) have hot dry summers and mild winters. Irrigated alfalfa is cultivated in all three areas.

METHODS

Despite underpinning biology common to all strains (Figure 1), the vital rates of strains may vary widely. Strain biology and the effects of weather on their vital rates are captured as biodemographic functions (BDFs, see below) and used to parameterize the PBDMs based on the time-invariant distributed maturation time population dynamics model (Abkin & Wolf, 1976; Manetsch, 1976) (see Appendix). PBDMs fall under the ambit of weather-driven time-varying life tables (Gilbert et al., 1976; Gutierrez, 1996).

Biodemographic functions

The biodemographic functions were estimated from extensive published laboratory age-specific life table data in Levi-Mourao et al. (2021, 2022) for strain *S*, and from Zahiri et al. (2010a, 2010b) for strain *I*. The data used to develop the original *E* strain model were more limited (Butler & Ritchie, 1967; Gutierrez et al., 1976). The available data are summarized in Table 1 and in the figures below. The data often did not cover the full range of relevant temperatures, and to avoid unrealistic estimates, the data were fitted using iterative methods in Microsoft Excel with the goodness of fit evaluated by regressing fitted to observed values. The fitted functions are given in each figure.

Developmental times and rates

The development time of ectotherms in days ($d(T)$) varies primarily with temperature (T) but may be influenced by nutrition and other

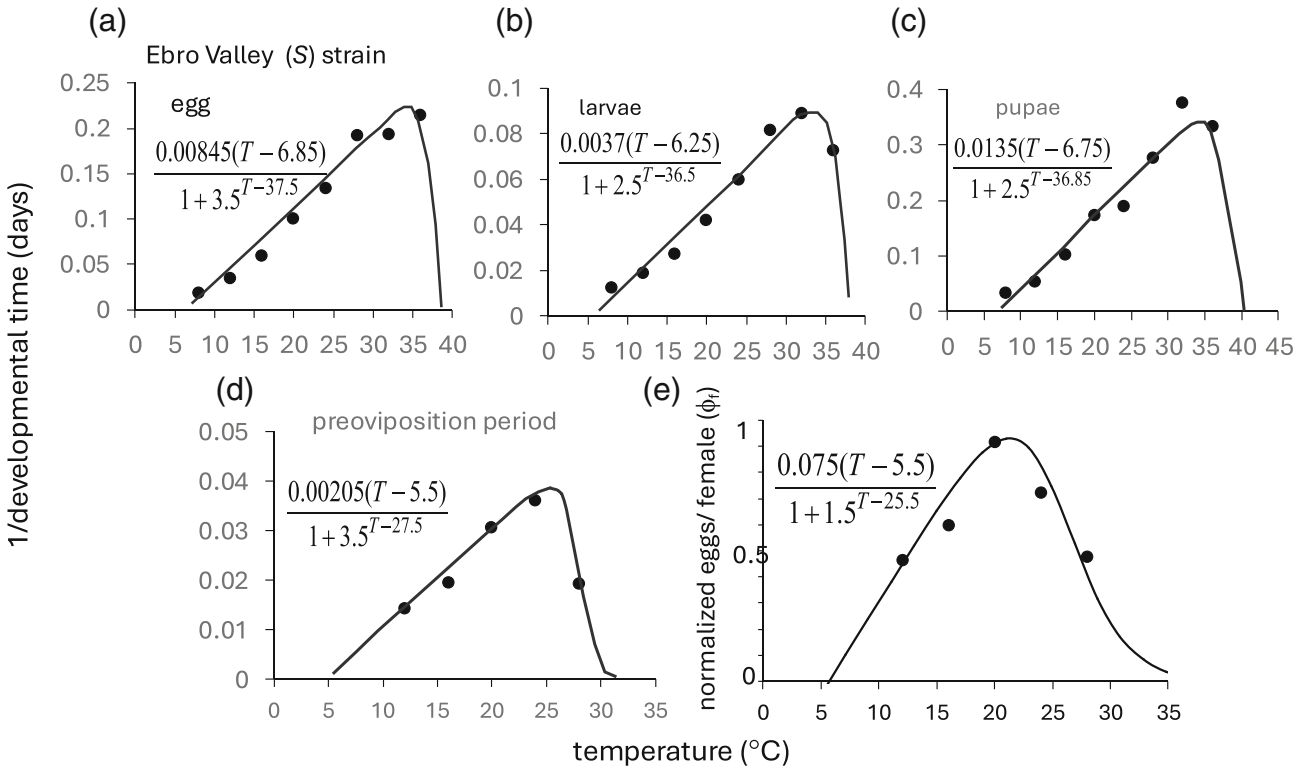

FIGURE 2 Developmental rates for the Ebro Valley *S* strain life stages: (a) eggs, (b) larvae, (c) pupae, (d) preoviposition period and (e) normalized oviposition rate (i.e., eggs female^{-1} d^{-1}) (data from Levi-Mourao et al., 2021, 2022)).

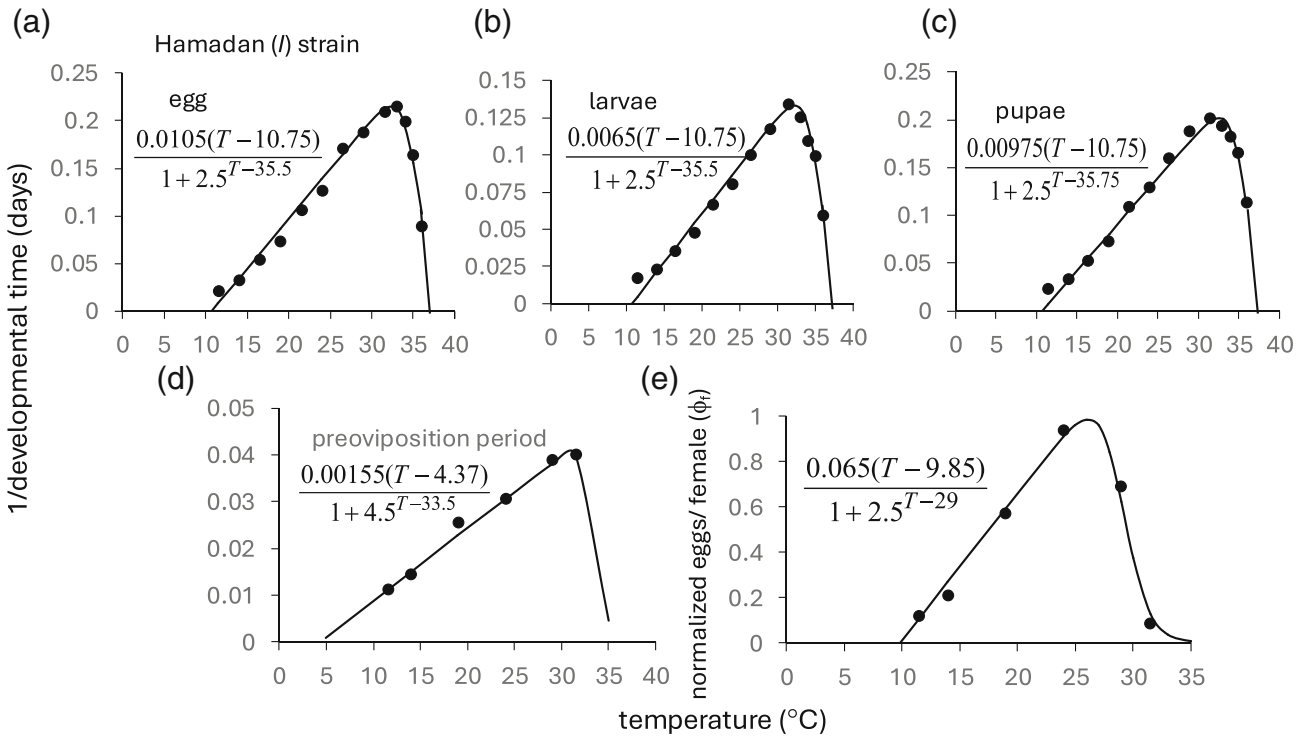

FIGURE 3 Developmental rates for the Hamadan *I* strain life stages: (a) eggs, (b) larvae, (c) pupae, (d) preoviposition period and (e) normalized oviposition rate (i.e., eggs female^{-1} d^{-1}) (data from Zahiri et al., 2010a, 2010b).

factors (Gutierrez, 1996). The developmental rate of a stage ($1/^{s}d(T)$ with left superscript s) across temperatures is estimated by a simple nonlinear model fit to laboratory data (Equation 1, see Figures 2 and 3)

$$^{s}R(T) = 1/^{s}d(T) = \frac{a(T-\theta_L)}{1+b^{T-\theta_U}}, \quad (1)$$

where a and b are constants, θ_L is the lower temperature threshold at $^{s}R(T) = 0$ and θ_U is the approximate upper inflection point where the rate of development begins to depart from linearity that, with increasing temperatures, declines to zero (see also Briére et al., 1999). Each data point in Figures 2 and 3 was estimated from a single life table conducted at a specific temperature.

The physiological developmental time constant ($^{s}\Delta$) of a stage in degree days ($dd > {}^{s}\theta_L$) was estimated in the linear range of favourable temperatures as $^{s}\Delta = d(T) \times (T - {}^{s}\theta_L)$ (Campbell et al., 1974). The daily increment of physiological time/age at time t is computed as $^{s}\Delta_x(T(t)) = {}^{s}R(T(t))^{s}\Delta$. The time step in the model is a day that from the perspective of the ectotherm weevil may vary greatly in physiological time units (i.e., $^{s}\Delta_x(T(t))$). On average, a cohort initiated at t_0 completes development when $\int_{t_0}^{t} {}^{s}R(T(t))dt = 1$ in continuous form, or $\sum_{t_0}^{t} {}^{s}\Delta_x(T(t)) = {}^{s}\Delta$ in our discrete time-invariant distributed maturation time dynamics model. Developmental times of cohort members have an Erlang distribution centered on $^{s}\Delta$ (Manetsch, 1976; see Appendix). Mean stage developmental times and thresholds for the three strains are summarized in Table 1.

Figures 2 and 3 summarize the developmental rate data for the egg, larval, pupal and preoviposition stages of the Ebro Valley (*S*) and Hamadan (*I*) strains, respectively. The lower thermal thresholds for the egg, larval and pupal stages of strain *S* are in the range ~ 7.25–7.75°C, while the preoviposition stage threshold is 5.5°C (Figure 2a–d respectively). The lower thresholds of *I* strain stages are in the range ~ 9.9–10.75°C, while the threshold for the preoviposition stage is 4.37°C with an oviposition threshold of 9.85°C (Figure 3a–e respectively). The rate of development of the egg, larval, and pupal stages of both strains decreases above ~32°C. The adult preoviposition developmental rate of the *S* strain begins to decline at about ~25°C, while that of the *I* strain begins to decline at ~29°C (Figure 2d vs. 3d). The upper thermal threshold for the two strains is ~38°C. The preoviposition developmental rate is used to compute daily aging in mature adults.

Aestivation

Most new spring–summer adults enter aestivation (i.e., summer-winter dormancy) in response to increasing photoperiod (dl >12 h, Figure 1b) (Bland, 1971; Ohto, 1996; Rosenthal & Koehler, 1968; Schroder & Steinhauer, 1976). The time of 12 h dl varies with latitude and is a critical component in local weevil phenology and dynamics. To develop the aestivation sub-model, 12 h dl is bracketed by ±0.5 h.

Specifically, during the fall to spring period as day length declines below 12.5 h and if adult physiological time $^{A}\Delta_x > 0$, a proportion of aestivating adults ($0 \le {}^{Out}\varphi(t) < 1$, Equation 2) terminate aestivation and begin preoviposition development leading to reproductive adults (Figure 1b).

$$\begin{aligned} &\text{if } dl(t) \le 12.5h \text{ and } {}^{A}\Delta_x > 0, \text{ then } 0 \le {}^{Out}\varphi(t) = 12.5h - dl(t) \le 1, \\ &\text{else } {}^{Out}\varphi(t) = 0 \end{aligned} \quad (2)$$

Upon completion of the preoviposition period during the fall to late spring period, females begin ovipositing in dry and green alfalfa stems, and upon hatching, the larvae feed on foliage, culminating in the production of new spring–summer adults.

However, in response to increasing daylength >11.5 h, a proportion of the new adults ($0 < {}^{In}\varphi(t) < 1$) enter dormancy each day during the hot summer—winter period (Equation 3)

$$\begin{aligned} &\text{if } dl(t) > 11.5h \text{ then } 0 \le {}^{In}\varphi(t) = (dl(t) - 11.5h) \le 1, \\ &\text{else } {}^{In}\varphi(t) = 0. \end{aligned} \quad (3)$$

New adults not entering aestivation ($0 < 1 - {}^{In}\varphi(t) < 1$) begin preoviposition development and at maturity may produce a second summer generation. These two simple rules (Equations 2 and 3) capture the aestivating biology in the three strains. Further, reproductive adults may cease ovipositing during summer when average temperatures consistently exceed the upper oviposition threshold (see below) and may over winter.

Reproduction

The life table studies used to summarize alfalfa weevil life stage developmental rates provided data on average physiological age (x) specific per capita oviposition rates (Figure 4a–c). Total oviposition ($F(t,T)$) by all females in the populations at time t and temperature T is computed as

$$F(t,T) = \left[0.5 \cdot \phi_E(T) \int_{x=1}^{x_{max}} f(x, T_{opt}) N(x,t) dx\right] \cdot {}^{A}\Delta_x, \quad (4)$$

where $f(x, T_{opt}) = \frac{e(x-d)}{1+c^{x-g}}$ is the per capita profile of eggs female^{-1} dd^{-1} at age (x) at approximately the optimum temperature (T_{opt}) with constants (c, d, e, g), the concave function $0 \le \phi_E(T) \le 1$ scales reproduction at non-optimal temperatures (Figures 2e and 3e), $N(t) = \int_{x=0}^{x_{max}} N(x,t)dx$ is the total number of adults, 0.5 is the proportion of females, and $^{A}\Delta_x(T(t))$ is the changes in physiological age (time). The threshold temperature for egg maturation and the preoviposition period are the same in the *S* strain (Figure 2d,e) but differ in the *I* strain (3 d, e). The minimal temperature for oviposition of strains *S* and *I* are respectively ~5.5°C and ~ 9.85°C, the optimal temperatures for the maximum oviposition d^{-1} are ~22°C and ~ 26°C, and the upper limits are ~31°C and ~ 32°C (Figure 4d). The minimum and

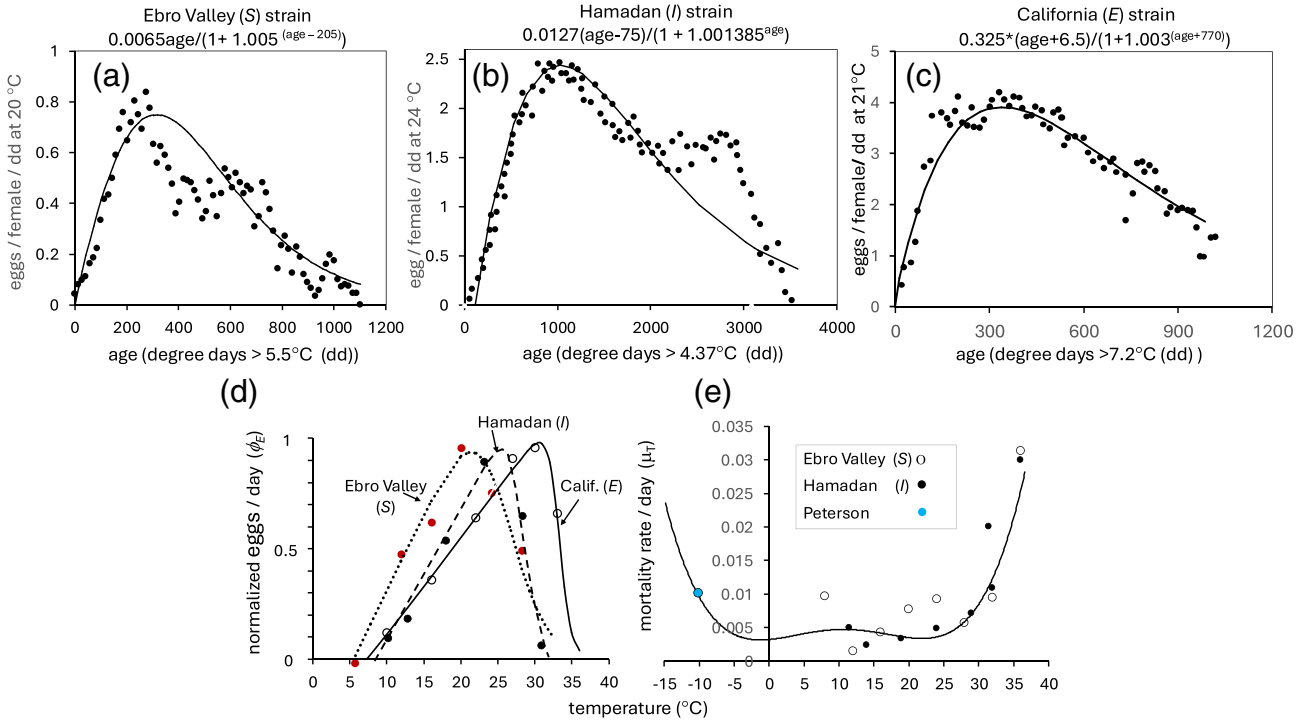

FIGURE 4 Biodemographic functions for three strains of alfalfa weevil: Oviposition profile of eggs female^{-1} dd^{-1} on age at the optimum average temperature (T_{opt}) for (a) the Ebro Valley *S* strain at 20°C, (b) the Hamadan *I* strain at 24°C and (c) the California *E* strain at 21.1°C which is below the optimum of ~30°C (see correction in the text); (d) the normalized eggs per female per day ($\phi_E(T)$) on temperature, and (e) the composite intrinsic adult mortality rate per day ($^A\mu_T(T)d^{-1}$) from the *S* and *I* strains data at mean temperatures plus the extreme value at −10°C from Peterson (1960, see text). The data for the *S*, *I* and *E* strains are, respectively, from Levi-Mourao et al. (2021, 2022), from Zahiri et al. (2010a, 2010b) and from Butler and Ritchie (1967) and Gutierrez et al. (1976). Values for all data were estimated from published figures and tables.

optimal temperatures for oviposition in the California *E* strain are ~7.2°C and ~30°C with an upper maximum of ~35°C (Gutierrez et al., 1976). The available oviposition profile for the *E* strain is at 21.1°C (Figure 4c) that is below the optimum of ~30°C (Figure 4d), and hence, $1.67\phi_E(T)$ corrects for this in Equation 4. The average total fecundities of *S*, *I* and *E* females under laboratory conditions are approximately 500, 3600 and 3000 respectively (Figure 4a–c).

Temperature-dependent mortality rate ($^s\mu_T(T)d^{-1}$)

All life stages occur in the field during summer, but only aestivating adults and eggs overwinter, and both stages are tolerant of freezing temperatures. Stage-specific daily mortality rates as a function of mean temperature ($^s\mu_T(T)d^{-1}$) were estimated as the slope in the midrange of the life table survivorship curves ($lx(T) \sim 0.5$). $^A\mu_T(T)d^{-1}$ data for the *S* strain are similar to the *I* strain data but are more variable. However, data at low temperature extremes were estimated from other sources and proved highly variable. For example, weevil adults collected in the field at different times were exposed to temperatures ranging from −5 to −15°C for 24 h and had average super cooling points ranging from −14.4 ± 0.7°C in October to −8.7 ± 0.4°C in May due to changes in seasonal levels of cryoprotectants (e.g., isorbitol, glycerol, glucose and trehalose) (Saeidi & Moharramipour, 2017). Using the January data, the mortality rate was $\sim 0.9d^{-1}$ at −10°C (i.e., $\sim 0.09/dd_{<0^\circ C}$). In contrast, Peterson (1960) exposed aestivating adults from Alberta, Canada and Utah, USA, to −10°C for different periods and found the two strains had similar mortality rates $0.01d^{-1}$ (i.e., $0.001/dd_{<0^\circ C}$). This rate is considerably lower than estimated by Saeidi and Moharramipour (2017) who further noted that actual temperatures experienced in overwintering refuges are likely higher.

Hence, as an initial estimate, a polynomial function was fitted to the *S*, *I* and Peterson data (Figure 4e, Equation 5). Sufficient digits are given to ensure accurate replication by others, and the function was extrapolated to temperatures < −10°C.

$$0.0025 \le {}^A\mu_T(T)d^{-1} = 0.0000001T^4 - 0.0000035T^3 + 0.0000293T^2 + 0.0001172T + 0.0039875 \le 1 \quad R^2 = 0.86,\ df = 16 \tag{5}$$

Morrison and Pass (1974) exposed four developmental age categories of eggs to −15, −20.5 and −23.3°C for periods of one to eight days. The older egg stage had begun embryonic development and was highly susceptible to cold, hence it was not used to estimate $^E\mu_T(T)d^{-1}$. The data at −15°C were consistent and at −15°C predicted $\sim {}^E\mu_T(T = -15^\circ C)d^{-1} = 0.186$ (i.e., $0.0124dd^{-1}$). These data

combined with data for the *I* strain data at non-freezing temperatures yield convex Equation 6.

$$0.0025 \le {}^{egg}\mu_T(T)d^{-1} = 0.0000004T^4 - 0.0000212T^3 + 0.0003396T^2 - 0.0010359T - 0.0028848 \le 1 \quad R^2 = 0.984, \quad df = 13 \tag{6}$$

Similar mortality functions for summer populations of the larval and pupal stages were developed at non-freezing temperatures from the life table data for strains *S* and *I*.

Density-dependent regulation

In an extensive study on density-dependent regulation in alfalfa weevil at Hamadan, Iran, Zahiri et al. (2014) found that only larval mortality caused by the entomopathogenic fungus, *Zoophthora phytonomi* (Arthur) Batko acted in a density-dependent manner. Larval instars III-IV were also attacked at low levels by the parasitoids *Bathyplectes curculionis* (Thomson) and *B. anurus* (Thomson) (Hymenoptera: Ichneumonidae), but density-dependent action could not be demonstrated. Only weevil larvae and adults feed on alfalfa foliage causing intra- and inter-stage competition. The non feeding egg and pupal stages are assumed not affected. To capture direct density-dependent mortality in larvae, a conservative composite function (${}^{L}\mu_N$, Equation 7) is used.

$${}^{L}\mu_N(T(t)) = 1 - e^{-c \cdot {}^{L}N(t) \cdot {}^{L}\Delta_x(T(t))} \tag{7}$$

An arbitrary constant $c = 0.0001$ is assumed, ${}^{L}N(t) = \int_{x=0}^{max} {}^{L}N(x,t)dx$ is larval density at time *t*, and ${}^{L}\Delta_x(T(t))$ is the increment of physiological time for larvae at temperature *T*(*t*).

Weather data

The weather data used to run the PBDM are from AgMERRA (Ruane et al., 2015), a global dataset for the period 1980–2010 consisting of a reanalysis of weather observations combined with observational datasets from in situ observation networks and satellites (https://data.giss.nasa.gov/impacts/agmipcf/). AgMERRA was selected because it is an established dataset developed by the Agricultural Model Intercomparison and Improvement Project (AgMIP, https://agmip.org/) providing daily, high-resolution, meteorological data designed for agricultural modelling applications. Compared with similar datasets, AgMERRA includes a substantially improved representation of daily precipitation distribution and extreme events, with relative humidity pegged to the time of maximum temperature, allowing for a more accurate representation of the diurnal cycle of near-surface moisture (Ruane et al., 2015). The AgMERRA daily weather data have a ~ 25 km spatial resolution for each of the 17,791 lattice cells for the Euro-Mediterranean region and 15,843 lattice cells for the United States, Mexico and Central America. Daily weather (max-min temperatures, solar radiation, mm rainfall, relative humidity) for the period 1 January 2000 to 31 December 2010 was used to run the PBDM across all lattice cells. Subsets of weather data were used to simulate site-specific dynamics.

GIS mapping

The PBDM predicts daily age-structured dynamics in all lattice cells (Figures 5 and 6), but only yearly georeferenced summary variables written to year-specific text files were used in mapping. Data from the first year when the model is assumed to be equilibrating was omitted in calculating means, standard deviations and coefficients of variation for all cell variables. Only mean values are reported here.

The open-source geographic information system (GIS) GRASS (2022), https://grass.osgeo.org; Neteler et al. (2012) GRASS version 8.3.1 was used for mapping using bi-cubic spline interpolation of the data on a 3-km raster grid that matched the resolution of the underlying digital elevation data. The interpolated PBDM raster maps were overlaid on base map layers using Natural Earth free data (https://www.naturalearthdata.com/). The digital elevation model is the public domain NOAA Global Land One-km Base Elevation (https://www.ngdc.noaa.gov/mgg/topo/globe.html). Only data below 2000 m asl were mapped. The geographic distribution of alfalfa cultivation is widespread in the Euro-Palearctic compared with the Nearctic (Tang et al., 2024), hence only the simulation data for areas of the Nearctic were masked.

RESULTS

As a guide, we first examine the prospective daily dynamics per m^2 of alfalfa for strains *S* and *I* using site-specific max-min temperatures, mm rainfall and hours daylength during years 2006–2010 (Figures 5a and 6a). Next, we simulate prospectively the geographic distribution and relative abundance of the three strains (*S*, *I*, *E*) across the Euro-Palearctic region, the United States, Mexico and Central America using 2000–2010 weather data. Lastly, the stabilizing adaptation of the *S* and *I* strains to weather in their native regions is explored.

Location-specific dynamics

The weather data used to run the Ebro Valley *S* strain model is summarized in Figure 5a. As observed in the field (Levi-Mourao et al., 2022), adult weevil oviposition may begin during late fall, with egg and larval populations occurring in late winter during some years (Figure 5b). Pupal stage dynamics are not illustrated. The phenology of adult entry to and exit from aestivation (Equations 2 and 3) is depicted in Figure 5c, with the transition periods in all years occurring at the same time in response to the critical one-hour day length window. The data in the figure are but part of the variables computed for each lattice cell.

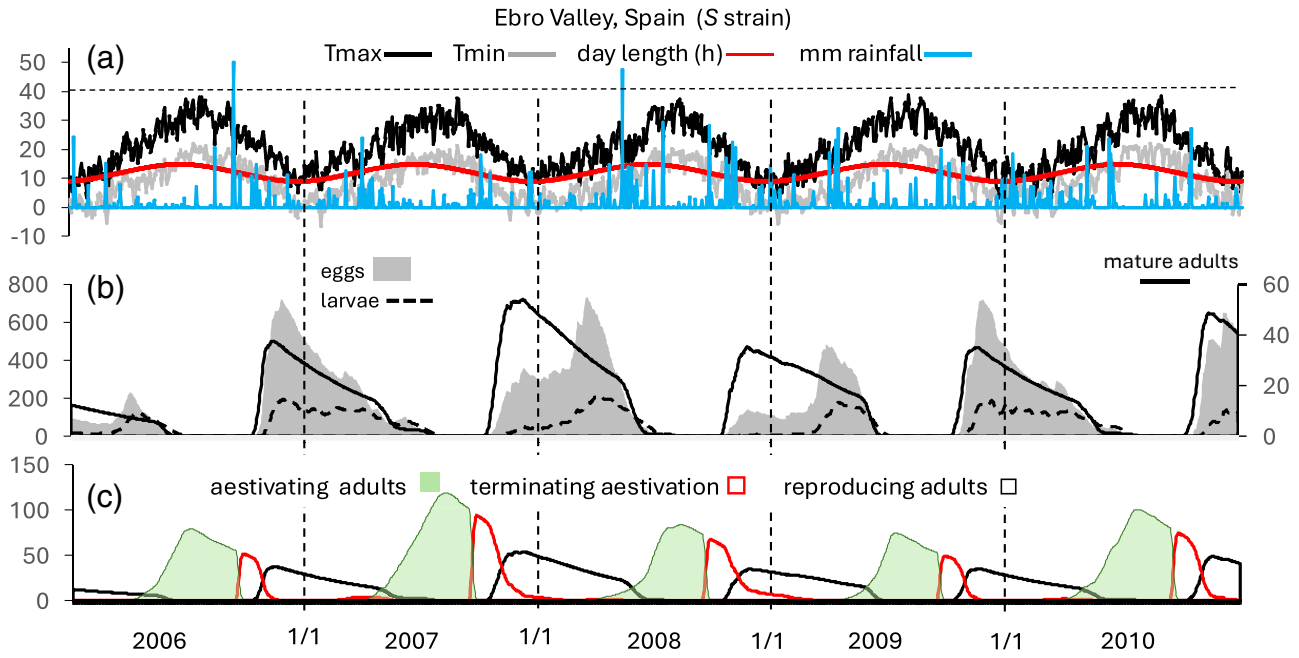

FIGURE 5 Simulated daily dynamics of Ebro Valley weevil *S* strain m^{-2} using weather data from Lleida, Ebro Valley, NE Spain (1/1/2006–12/31/2010): (a) daily values of maximum and minimum temperature (°C), mm rainfall and hours daylength; (b) the average number of eggs, larvae (left scale) and adults (right scale); and (c) the dynamics of new adults entering aestivation, terminating aestivation and becoming reproductive adults.

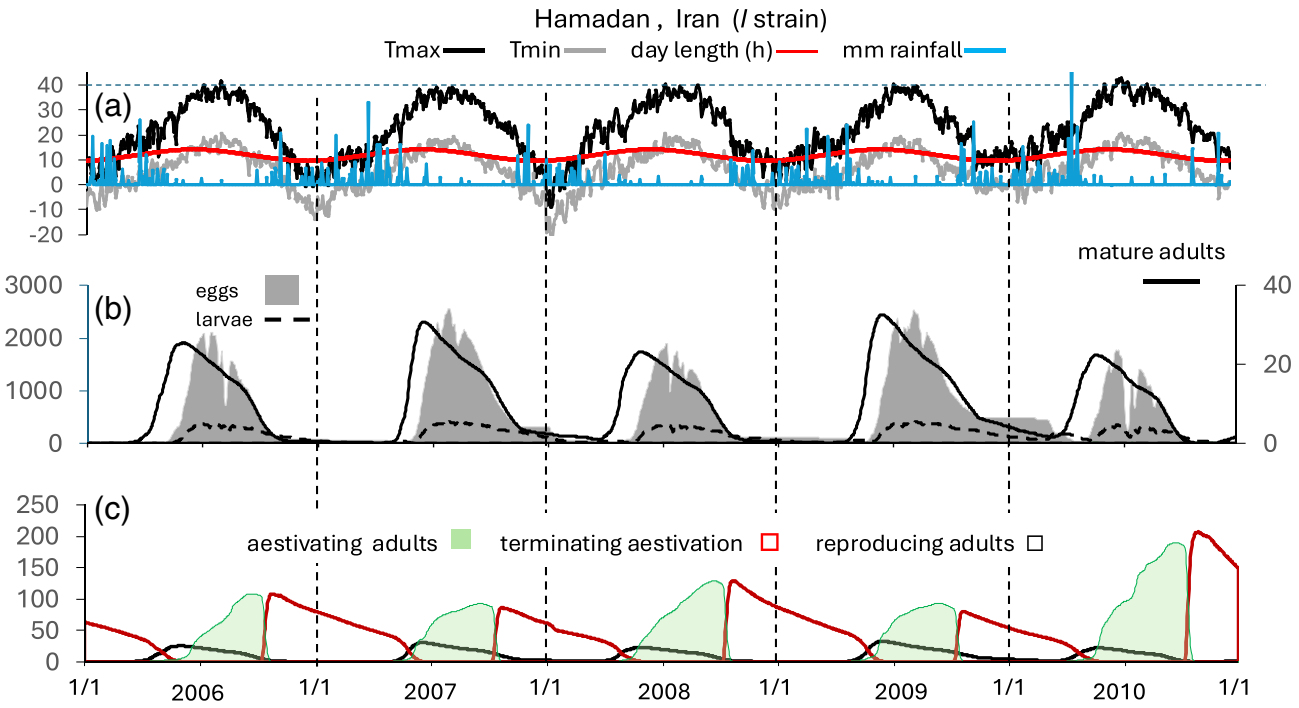

FIGURE 6 Simulated daily dynamics of the Hamadan *I* strain alfalfa weevil m^{-2} using Hamadan, Iran weather data (1/1/2006–12/31/2010): (a) daily values of maximum and minimum temperature (°C), mm rainfall and hours daylength; (b) the average number of eggs, larvae (left scale) and adults (right scale); and (c) the dynamics of new adults entering aestivation, terminating aestivation and becoming reproductive adults.

Hamadan, Iran temperatures (Figure 6a) may exceed 40°C during summer, and minimum temperatures may fall below −10°C during winter (e.g., 2007–2008). The dynamics of the Hamadan *I* strain are illustrated in Figure 6b,c showing that high summer temperatures and cold fall–winter weather restrict oviposition mostly to the spring–summer period. Outbreaks of the weevil may occur in Iran after mild

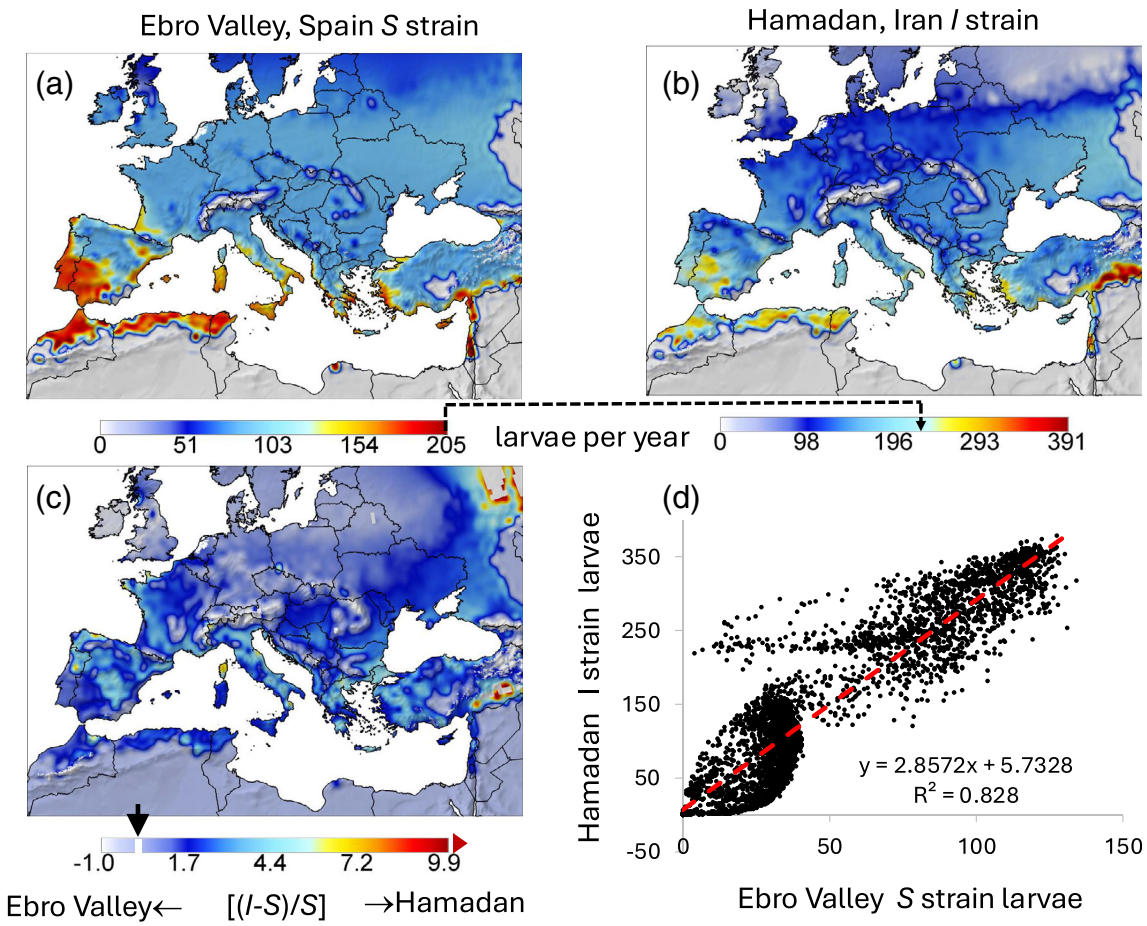

FIGURE 7 Simulated prospective average cumulative alfalfa weevil larvae m^{-2} per year using weather data from 2000 to 2010 for the Euro-Palearctic region below 2000 m asl: (a) Ebro Valley *S* and (b) Hamadan *I* strains, (c) map of the relative larval abundance of the *I* strain relative to the *S* strain (i.e., $[(I-S)/S]$) clipped at 10 with the broad white line in the colour bar indicating the zero value, and (d) the relationship of cumulative *I* strain larval densities to cumulative *S* larval densities across all locations. In North Africa and the Middle East, >350 mm rainfall/year is used to define the limits of alfalfa growth except under irrigation (not shown). Alfalfa is widely grown in Europe (c.f., Tang et al., 2024) and hence masking was not performed. The dash line arrow between a to b indicates equal values.

winters (Saeidi & Moharramipour, 2017) as seen in the development of high numbers of aestivating adults in late 2010 due to relatively mild late summer–fall weather.

Geographic distribution and abundance

Euro-palearctic region

The georeferenced simulation data are mapped below 2000 m asl, accounting for apparent gaps in the maps (e.g., the Alps). Prospectively, annual larval densities of the Ebro Valley *S* strain are lower than the Hamadan *I* strain across the Euro-Palearctic region (Figure 7a vs. b) with both strains being more abundant in warmer areas. Note the high densities in the Ebro Valley in NE Spain (Figure 7a). As a reference, the dashed arrow above the colour bars indicates equivalent densities of the two strains. The S strain is prospectively more uniformly distributed in northern areas. The difference in the distribution of abundance is illustrated as the strain larval density ratio $(I-S)/S$ computed for each lattice cell (Figure 7c) and by the regression showing the *I* strain is ~2.8 times more abundant than the *S* strain (Figure 7d).

Invasive potential of the *S* and *I* stains in the Nearctic

Using the same nominal initial conditions as in Figure 7, the simulated geographic distribution and relative cumulative annual abundance of *S* and *I* strain larvae in the United States, Mexico and Central America masked for alfalfa cultivation are summarised in Figure 8a,b respectively. The area with favourable temperatures in the southwest United States is much larger than the area masked for cultivated alfalfa.

Prospectively, the *S* strain has ~25%–50% lower densities across the regions than the *I* strain suggesting a lower invasiveness potential. The *I* strain is predicted most abundant in the hot area of California and Arizona where the Egyptian strain was first detected, but

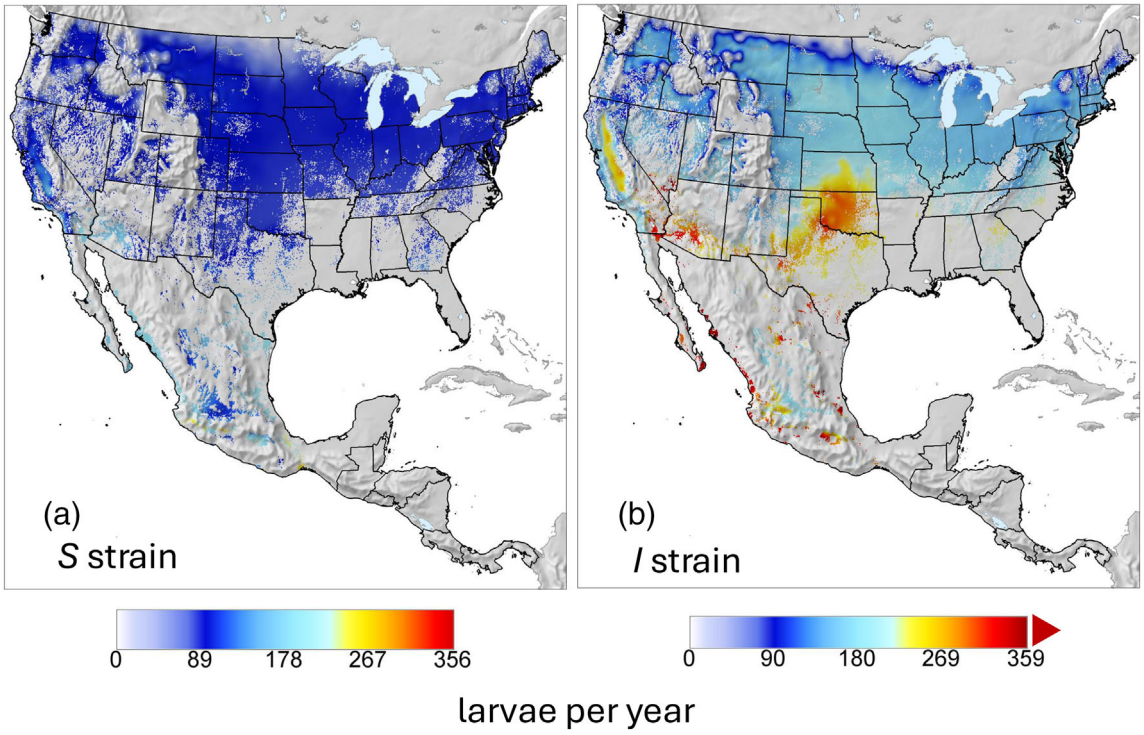

FIGURE 8 Simulated prospective average cumulative number of alfalfa weevil larvae m^{-2} per year utilizing weather data from 2000 to 2010 in the United States, Mexico, and Central America below 2000 m asl and masked for area of alfalfa cultivation (c.f., Tang et al., 2024): (a) Ebro Valley *S* strain and (b) Hamadan *I* strain clipped at 360.

relatively high densities are also predicted in the southern US plains with densities decreasing northward to below the Canadian border. Most alfalfa in Canada is grown in the provinces of Alberta, Saskatchewan and Manitoba beyond the limits of our study.

The lower preoviposition temperature threshold in the *I* strain (4.37°C) compared with the *S* strain (5.5°C) enables earlier reproduction in spring, and its higher optimum (~26.5°C vs. ~21°C) enables oviposition during hotter weather despite its higher minimum temperature for oviposition (9.85 vs 5.5 degrees) (Figure 4d). Further, the 7 to 8-fold higher fecundity and longer oviposition period of the *I* strain give it an added advantage.

Strain adaptation to local environments

Weather varies greatly across the weevil's Holarctic range, and strains occurrence has been amply documented (e.g., Bundy et al., 2005; Coles & Day, 1977; Sanaei & Seiedy, 2016; Schroder & Steinhauer, 1976; Tuda et al., 2021). The high variability of the vital statistics of strains *S*, *I* and *E* is summarized in Figure 9. The most interesting question is why fecundity in the *S* strain is ~7-8-fold less than that of the *I* and *E* strains (~500 vs. ~3600, ~3000), and less than the averages of 4200, 3100 and 3250 eggs estimated for field-collected females in New Jersey, Kentucky and Indiana, respectively (see Coles & Day, 1977). The Levi-Mourao et al. (2021, 2022) studies on the *S* strain used sound experimental procedures and continually refreshed laboratory stocks with adults captured in different fields to reduce inbreeding and selection for a laboratory strain. The excellent studies by Zahiri et al. (2010a, 2010b) on the *I* strain were similarly rigorous. Hence, the obvious question to explore is whether the differences in fecundity are adaptations to conditions in their native environments.

Gilbert (1986; see Gilbert et al., 2010) opined that '*The ecological notion of density-dependence implies that, as population density increases, there will be a corresponding decline in the survival or reproduction of the population as a whole … there must be some mechanism-ecological or genetical-which restricts individual fecundity to the level appropriate to the population as a whole*'. To explore this and specifically why the difference in fecundity of the *S* and *I* strains is so large, we examine what would happen if the observed fecundity of both strains was increased or decreased keeping all other vital rates unchanged (*c.f.*, Gilbert, 1986).

A critical aspect of the weevil's biology is survival during the adverse periods when hosts may be lacking and/or when weather becomes too hot or too cold for reproduction (see Marshall et al., 2020). Such periods are bridged by aestivating adults (^{aes}A), and hence, the annual production of ^{aes}A is used as our metric of stabilizing selection. Weather affects weevil vital rates, density-dependent mortality ($^{L}\mu_N$, Equation 7) limits larval density, and adult temperature-dependent mortality ($^{A}\mu_T$) is density-independent.

Using 2006–2010 Ebro Valley weather and multiples ($\phi_f = [0.1, 0.5, 1, 1.5, 2, 3, 4, 5, 6, 7]$) of observed *S* strain fecundity (ϕ_f *F*,

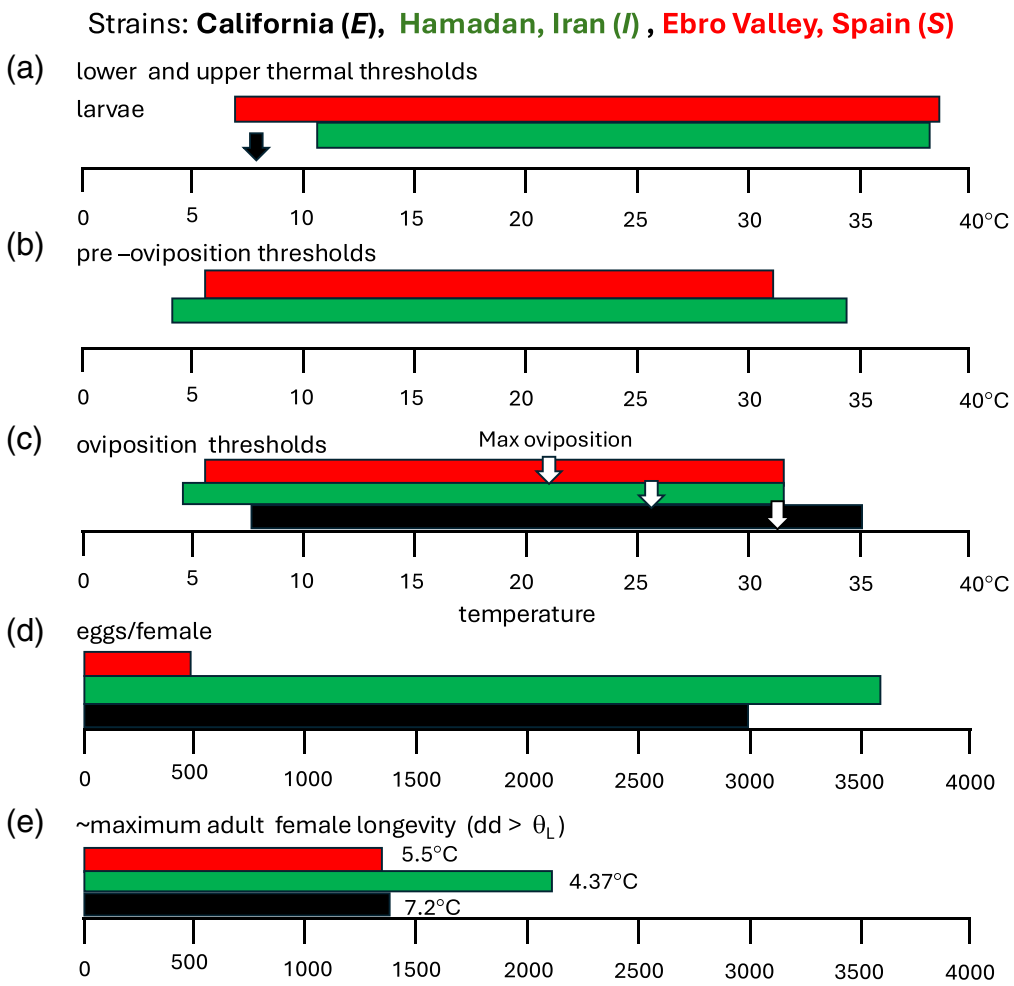

FIGURE 9 Comparison of alfalfa weevil strains traits: (a) larval thermal thresholds with the black arrow indicating the lower thermal threshold of the *E* strain, (b) thermal limits for preoviposition development, (c) thermal limits for oviposition with temperature for maximum oviposition in each strain indicated by open arrows, (d) total fecundity per female at the optimum temperature and (e) approximate mean adult female longevity in degree days above the lower preoviposition threshold indicated next to bars. The black arrow in 9a is the lower thermal threshold of the California *E* strain.

Equation 4), simulated maximum ${}^{aes}A$ occurs near observed fecundity (i.e., $\phi_f \sim 1$, Figure 10a) while larval survival decreases with increasing ϕ_f (Figure 10b). Using Ebro Valley weather for the *I* strain but scaling its high fecundity by ϕ_f = [0.1, 0.25, 0.5, 0.75, 1.0, 1.5, 2, 3], maximum ${}^{aes}A$ occurs near $\phi_f = 0.1$ (Figure 10c). This suggests that under Ebro Valley conditions, the ~7-8-fold higher fecundity of the *I* strain would be largely wasted due to density-dependent mortality, and by extension, selection for lower fecundity should occur as anticipated by Gilbert (1986) and Gilbert et al. (2010).

Using Hamadan weather for the *I* strain, and applying ϕ_f = [0.1, 0.25, 0.5, 0.75, 1.0, 1.5, 2, 3] to scale fecundity while keeping the same density-dependent mortality model (${}^{L}\mu_N$), maximum average ${}^{aes}A$ still occurs at $\phi_f \sim 0.1$ (Figure 10d). This arises because ${}^{A}\mu_T(T)$ is based on average temperatures and has a small range (e.g., $\sim 0.0025d^{-1} < {}^{A}\mu_T(T) < \sim 0.03d^{-1}$, Equation 5) resulting in low adult winter mortality compared with the impact of density-dependent mortality (${}^{L}\mu_N$). To explore this interaction, we examine the joint effects on ${}^{aes}A$ in the *S* and *I* strains of scaling both temperature-dependent adult mortality (i.e., $\phi_T {}^{A}\mu_T$) and fecundity ($\phi_f F$) given the effects of ${}^{L}\mu_N$.

Effects of ($\phi_T {}^{A}\mu_T, \phi_f F$) and ${}^{L}\mu_\rho$ on ${}^{aes}A$

Using Ebro Valley 2006–2010 weather and the *S* strain model, annual combinations of ($\phi_T {}^{A}\mu_T, \phi_f F$) were run to examine the effects on the production of ${}^{aes}A$. Specifically, fecundity ($F(t,T)$, Equation 4) was scaled by ϕ_f = [0.1, 0.25, 0.5, 0.75, 1, 1.5, 2, 3, 4, 5, 6, 7] and daily ${}^{A}\mu_T$ (Equations 5) was scaled by ϕ_T = [1, 2, 3, 4, 5, 6, 7]. Similarly, using the *I* strain model and Hamadan weather, high fecundity $F(t,T)$ was scaled by ϕ_f = [0.1, 0.25, 0.5, 0.75, 1, 2, 3] and ${}^{A}\mu_T$ was scaled by ϕ_T = [1, 2, 3, 4, 5, 6, 7, 8]. The simulation data are mapped in Figure 11 smoothing the surface to capture the average trends (MATLAB, The MathWorks Inc., 2022).

For strain *S*, maximum ${}^{aes}A$ follows the contour of the surface indicated by the dashed line arrow indicating maximization occurs

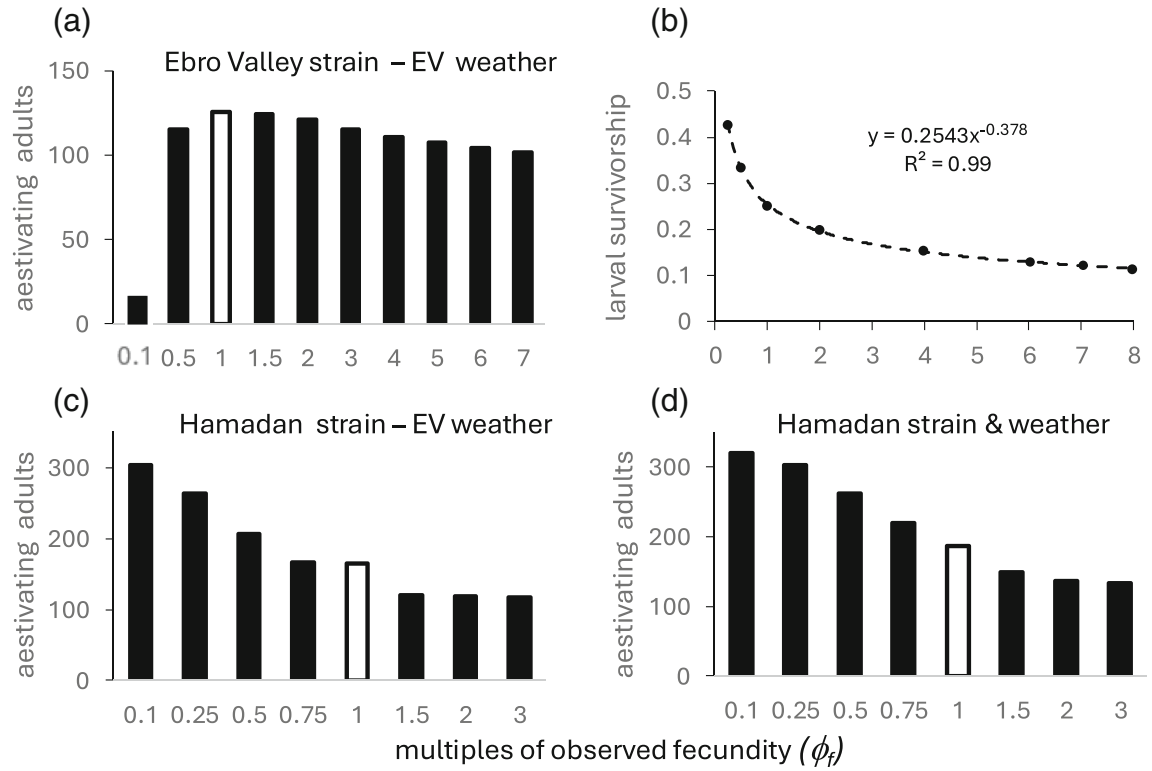

FIGURE 10 The effects of multiples of observed weevil strain fecundity (ϕ_f) on average aestivating adults (^{aes}A) per year during 2006–2010: (a) Ebro Valley *S* strain using Lleida, Spain weather (EV), (b) mean *S* strain larval survival on ϕ_f, (c) Hamadan *I* strain using Lleida, Spain weather (EV) and (d) Hamadan *I* strain ^{aes}A per year using Hamadan, Iran weather. The white bars indicate observed fecundity.

near [$\phi_f = 1$, $\phi_T = 1$] (black dot in Figure 11a,c), but as ϕ_T increases, ϕ_f must increase to achieve roughly the same level of ^{aes}A (i.e., Gilbert's prediction). This suggests a more limited invasive potential of the *S* strain into harsher climates.

In contrast, ^{aes}A for the Hamadan strain is not maximized at [$\phi_f \sim 1$, $\phi_T \sim 1$], but is maximized along a narrower ridge at $\phi_f \sim 1$ as $\phi_T \to 8$ (Figure 11b,d). Large increases in *I* strain fecundity ($\phi_f > 1$) are countered by increasing $^{L}\mu_N$, while $\phi_f < 1$ is grossly suboptimal. This results because $^{A}\mu_T$ (Figure 4e) was estimated using average laboratory temperatures that underestimate field mortality rates. However, multiplying $^{A}\mu_T$ by $\phi_T = 8$ is more in line with the mortality rate estimated in Iran by Saeidi and Moharramipour (2017). In contrast to Ebro Valley, daily field temperatures at Hamadan, Iran fluctuate to extreme highs during summer and extreme lows during winter (see Figure 6a) with concomitant increases in mortality. Further, the results suggest $^{A}\mu_T$ should be estimated and applied in the model on a shorter time interval (say hourly) to capture the effects of daily temperature fluctuations under extreme conditions.

The ~8-fold greater reproductive rate of the *I* strain compared with the *S* strain appears to a hedge against expected high levels of mortality, enabling maximum production of ^{aes}A to survive extreme low winter temperatures. The results suggest a tradeoff between high fecundity and high expected $^{A}\mu_T$ given expected $^{L}\mu_N$ (i.e., stabilizing selection, sensu Gilbert, 1986; Gilbert et al., 2010). Compared with the *S* strain, other attributes increasing ^{aes}A production in the *I* strain are its low preoviposition threshold (4.37°C) that enables earlier maturation of eggs in spring and a higher optimal oviposition temperature (~26.5°C) that enables greater oviposition during the hot summer. But how do these attributes affect strain invasiveness?

Strain invasiveness and adaptation

To examine invasiveness of the *S* and *I* strains under high levels of expected winter mortality of ^{aes}A across the Euro-Palearctic region, we use $\phi_T {}^{A}\mu_T$ where $\phi_T = 8$ for $T < 0$°C, and given observed $F(t,T)$ and $^{L}\mu_N$ (Figure 12a,b). While the *S* strain is optimal for the Ebro Valley at $\phi_T = 1$(see Figures 7a and 10a), its invasive potential regionally under the higher winter mortality rates is low, especially in the eastern Palearctic (Figure 7a vs. 12a). The density and distribution of the *I* strain are largely unchanged in western regions with a reduction of about 10% in warmer areas such as Spain and North Africa but greatly reduced and limiting densities in the eastern Palearctic (Figure 7b vs. 12b).

Using weather data for the United States, Mexico and Central America and masking the results for areas of alfalfa cultivation, the distribution of densities of all three strains is constrained northward by high winter mortality. However, the *I* and *E* strains are constrained less because of 7-8-fold higher $F(t,T)$ (Figure 12c–e). All three strains are predicted in the Great Central Valley of California, with *I* strain

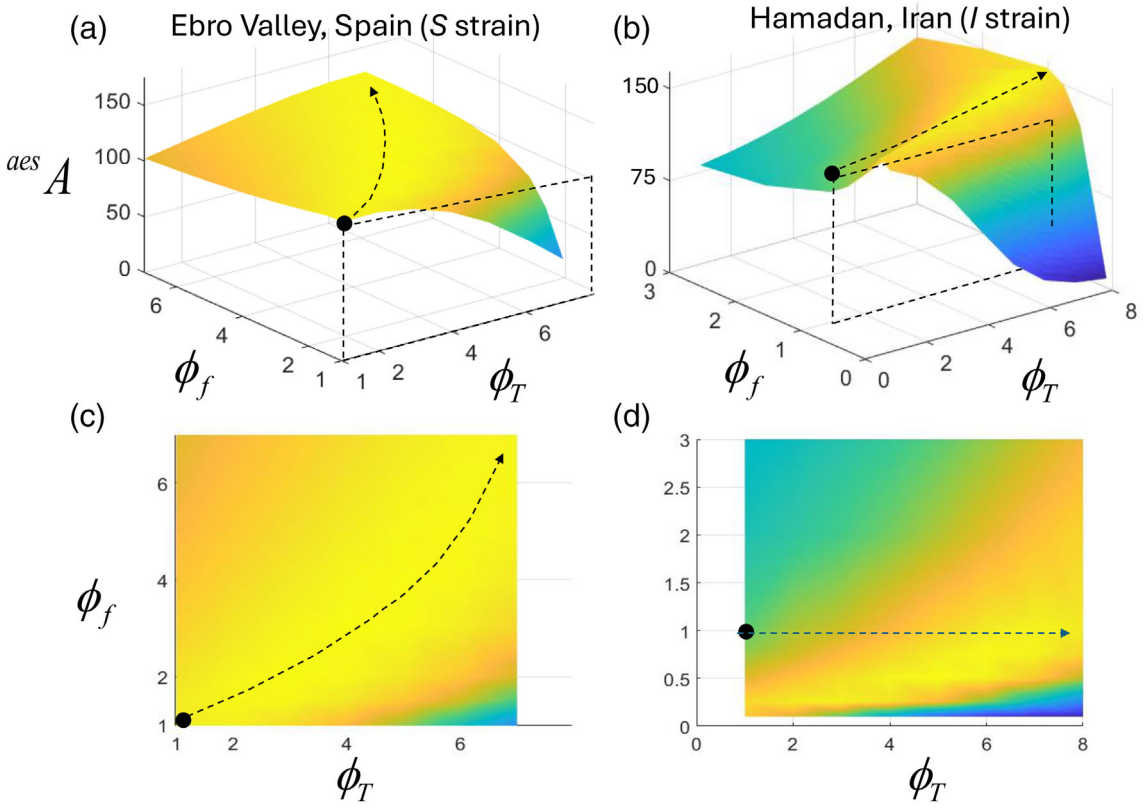

FIGURE 11 Average number of aestivating alfalfa weevil adults per year (^{aes}A) for the Ebro Valley (*S*) and Hamadan (*I*) strains using multiples of observed daily fecundity (ϕ_f) and multiples of daily temperature-dependent mortality rate (ϕ_T) using 2006–2010 weather: (a) Ebro Valley strain *S* and (b) Hamadan, Iran strain *I*. The dashed rectangles in the figures (a) and (b) indicate $\phi_f = 1$ across all ϕ_T. Subfigures (c) and (d) are surface plots of (a) and (b) data, respectively (MATLAB, The MathWorks Inc., 2022).

weevil densities being highest there and in known irrigated alfalfa in the hot desert areas of southern California and Arizona where freezing winter temperatures are rare, and in part of the central plains of the United States with harsh winters (Figure 12b). While the prospective distribution of the *E* strain is similar to the *I* strain, its larval densities are ~35% lower, suggesting the *I* strain is more invasive across the region. Sanaei et al. (2016) concluded that the western and Egyptian/eastern strains in the United States may have had their origins in climates like Iran. Further, adaptative changes in *E* strain vital rates likely occurred since its initial invasions of the United States in the late 1930s and the Gutierrez et al. (1976) study, with vital rate changes (Sanaei & Seiedy, 2016) not being detectable by the genomic analyses (Böttger et al., 2013; Sanaei et al., 2016).

DISCUSSION

Alfalfa weevil is an important invasive pest of alfalfa with origins in the Palearctic and numerous strains have been characterized genomically (e.g., Böttger et al., 2013; Bundy et al., 2005; Coles & Day, 1977; Sanaei et al., 2016; Sanaei & Seiedy, 2016; Schroder & Steinhauer, 1976; Tuda et al., 2021), but their invasiveness in novel environments has not been assessed demographically. Three strains having different current distributions invaded the United States (see Bundy et al., 2005) that are separable based on mitochondrial sequence data but cannot be separated using nuclear loci, suggesting that they recently diverged (Böttger et al., 2013).

To examine the invasiveness of weevil strains, PBDMs of their weather-driven population dynamics were developed. Specifically, the extensive life table data for weevil populations from the Ebro Valley in NE Spain (Levi-Mourao et al., 2021, 2022) and from Hamadan, Iran (Zahiri et al., 2010a, 2010b) were used to parameterize PBDMs for them. Because of their disparate vital rates, the populations are designated as strains *S* and *I*. The PBDMs were used to explore strain invasiveness in parts of the Palearctic and Nearctic. Our analysis shows that the vital rates of the *I* strain make it more invasive than the *S* strain, but its 7-8-fold higher fecundity would be wasted due to density-dependent mortality in many areas. The obvious question is why the large difference in fecundity occurs.

To explore this question we used Gilbert's (1986) theory that individual fecundity is selected to the level appropriate to the population in the native environment using annual aestivating adult production in response to varying levels of temperature-dependent mortality and observed per capita fecundity given density-dependent mortality as our metric (see Figure 11). While the results conformed to Gilbert's predictions, after invasion of a strain into a novel area, strain vital

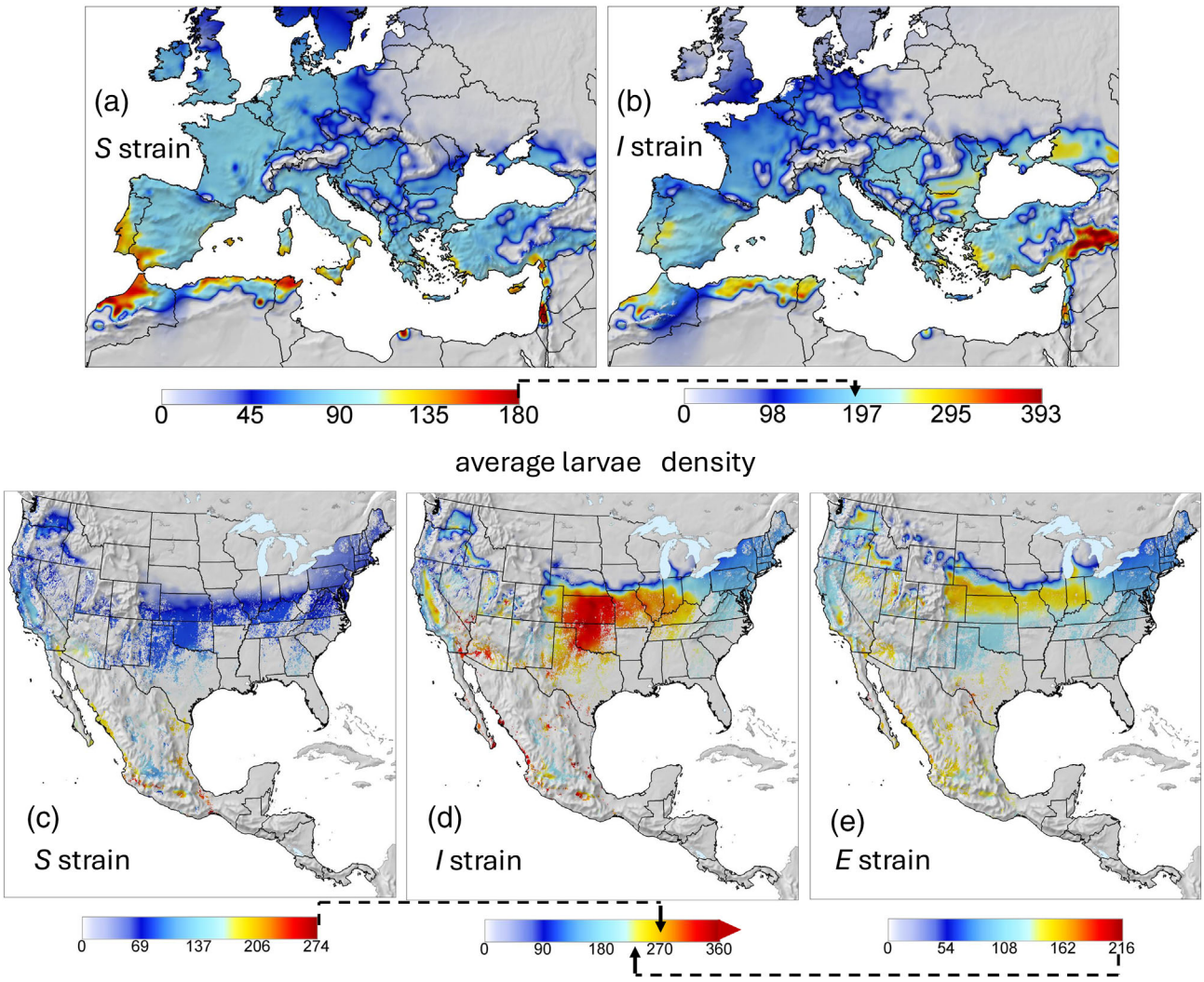

FIGURE 12 Average alfalfa weevil larvae per year for the Ebro Valley (*S*), Hamadan (*I*) and California (*E*) strains using observed daily fecundity ($\phi_f = 1$) and $\phi_T = 8$ fold the daily adult temperature-dependent mortality rate ($^A\mu_T$) using 2000–2010 weather <2000 m asl: (a) *S* strain and (b) *I* strain in the Euro-Palearctic region; (c) *S* strain, (d) *I* strain and (e) *E* strain in the United States, Mexico and Central America. The dashed line arrows between Figure 12a,b, Figure 12c,d and Figure 12d-e point to equal values. Data for the Nearctic regions were masked for the area of alfalfa cultivation (c.f., Tang et al., 2024).

rates would be expected to change in concert (see Figure 9 and Table 1).

The data for the supposed Egyptian *E* strain that invaded Arizona-California in the 1930s are less complete (Butler & Ritchie, 1967; Gutierrez et al., 1976), and unknown adaptations in the strain likely occurred during the five decades. Hence, analysis of *E* strain adaptation to Arizona-California conditions based on old data was not prudent. Evidence of possible adaptation in the western strain to local conditions comes from the Canadian prairies where its range and status as a minor pest in 2001 increased to become the principal pest of alfalfa by 2014 (https://canadianagronomist.ca/alfalfa-weevil-and-its-parasitoids; see Soroka et al., 2024). Adaptation in the weevil (and other invasive species) to novel environments has at least three components: adaptation to extant local climate, to abiotic and biotic characteristics of its new range, and dynamically to local climate change. Parsing these effects on a strain in a novel environment(s) could be accomplished by the development of a PBDM early in the invasion process with periodic updates of parameters to track the time course of adaptations. This is possible because PBDMs model the weather-driven biology to determine the extant and potential range—species presence data are not required but could be used for validation purposes. Further, in concert with genomic analyses, possible genomic changes could be discovered (e.g., Sanaei et al., 2016) that could help determine prospectively the geographic/climatic origins of an invasive species strain. In such studies, sound biological data underpinning the model is paramount.

Two recent examples of PBDMs predicting the correct invasive potential are for the South American tomato pinworm (*Tuta absoluta* (Meyrick) (Lepidoptera: Gelechiidae)) in the Euro-Palearctic region (Ponti et al., 2021) and the risk analysis of the invasive potential of the African false codling moth (*Thaumatotibia leucotreta* (Meyrick) (Lepidoptera: Tortricidae)) to Europe (EFSA PLH Panel et al., 2023).

PBDM can easily accommodate tri-trophic interactions (see Gutierrez & Ponti, 2013) and *ex ante* analyses would help guide the search for and introductions of biological control agents to improve the current low success rate of biological control programmes (Cock et al., 2016; Van Lenteren et al., 2006). For example, the tri-trophic PBDM system model of the coffee/coffee berry borer system in Colombia explained the failure of parasitoids introduced for its control and enabled developing recommendations for alternative pest management strategies (Cure et al., 2020). Biological control efforts for alfalfa weevil are ongoing in North America, and a tri-trophic model could include mating (Hsiao & Hsiao, 1985; Tuda et al., 2021) and host-parasitoid incompatibilities (Salt & van den Bosch, 1967), the action of fungal pathogens (Zahiri et al., 2014) and other issues (e.g., *Wolbachia* effects). The model could aid in the development of management strategies.

AUTHOR CONTRIBUTIONS

Andrew Paul Gutierrez: Conceptualization; data curation; formal analysis; funding acquisition; investigation; methodology; project administration; resources; software; supervision; validation; visualization; writing – original draft; writing – review and editing. **Luigi Ponti:** Data curation; funding acquisition; investigation; methodology; project administration; resources; software; validation; visualization; writing – review and editing. **Alexandre Levi-Mourao:** Data curation; project administration; validation; writing – review and editing. **Xavier Pons:** Data curation; funding acquisition; project administration; validation; writing – review and editing. **José Ricardo Cure:** Investigation; methodology; resources; validation; writing – review and editing. **Markus Neteler:** Software; writing – review and editing. **George Simmons:** Writing – review and editing.

ACKNOWLEDGEMENTS

We dedicate this paper to the memory of Mr. Neil E. Gilbert (deceased), Cambridge University, UK, who co-developed the concept of time-varying life tables and set the basis for the development of PBDMs. We thank authors Drs. E. Sanaei and B. Zahiri and Iranian colleagues for their excellent studies on alfalfa weevil that made the analysis possible. An anonymous reviewer and Assistant Editor C. MacQuarrie raised important questions that helped with the 5th Augean task of revising the manuscript. We are grateful to the international network of developers who maintain and continue to improve the Geographic Resources Analysis Support System (GRASS, https://grass.osgeo.org) GIS software and make it available to the scientific community. The study was supported by CASAS Global NGO (https://www.casasglobal.org), the McKnight Foundation (grant number 22-341 and 24-124) and project TEBAKA (project ID: ARS01_00815) co-funded by the European Union—ERDF and ESF, 'PON Ricerca e Innovazione 2014-2020'. The Spanish studies were funded by the Ministerio de Ciencia e Innovación of the Spanish Government (project AGL2017-84127-R). Open access publishing facilitated by ENEA Agenzia Nazionale per Le Nuove Tecnologie l'Energia e lo Sviluppo Economico Sostenibile, as part of the Wiley - CRUI-CARE agreement.

CONFLICT OF INTEREST STATEMENT

The authors have no conflicts of interest to declare.

DATA AVAILABILITY STATEMENT

The biodemographic functions were estimated from published laboratory age-specific life table data in Levi-Mourao et al. (2021, 2022) for strain S, from Zahiri et al. (2010a, 2010b) for strain I and from Butler and Ritchie (1967) and Gutierrez et al. (1976) for strain E (see Methods). The life table data should be requested from the authors of the cited papers. All the functions used in the model are present in the text and figures. All the data are available open access on Zenodo at https://doi.org/10.5281/zenodo.14914244.

ORCID

Andrew Paul Gutierrez https://orcid.org/0000-0001-7773-1715
Luigi Ponti https://orcid.org/0000-0003-4972-8265
Alexandre Levi-Mourao https://orcid.org/0000-0003-2310-6994
Xavier Pons https://orcid.org/0000-0002-0874-8449
José Ricardo Cure https://orcid.org/0000-0001-5816-0259
Markus Neteler https://orcid.org/0000-0003-1916-1966
George Simmons https://orcid.org/0000-0002-9076-4973

REFERENCES

Abkin, M.H. & Wolf, C. (1976) *Computer library for agricultural systems simulation. Distributed delay routines: DEL, DELS, DELF, DELLF, DELVF, DELLVF*. Lansing, MI, USA: Department of Agricultural Economics, Michigan State University.

Aḏkā'i, P. (2003) *Hamadān i. geography*, Vol. 11. New York, NY: Encyclopædia Iranica, pp. 595–599.

Baranowski, P., Krzyszczak, J., Slawinski, C., Hoffmann, H., Kozyra, J., Nieróbca, A. et al. (2015) Multifractal analysis of meteorological time series to assess climate impacts. *Climate Research*, 65, 39–52.

Biedrzycka, A., Fijarczyk, A., Kloch, A. & Porth, I.M. (2022) Editorial: genomic basis of adaptations to new environments in expansive and invasive species. *Frontiers in Ecology and Evolution*, 10, 974649.

Bland, R.G. (1971) Photoperiod-diapause relationships in the alfalfa weevil, *Hypera postica*. *Annals of the Entomological Society of America*, 64, 1163–1166.

Böttger, J.A.A., Bundy, C.S., Oesterle, N. & Hanson, S.F. (2013) Phylogenetic analysis of the alfalfa weevil complex (coleoptera: Curculionidae) in North America. *Journal of Economic Entomology*, 106, 426–436.

Briére, J.F., Pracros, P., Le Roux, A.Y. & Pierre, J.S. (1999) A novel rate model of temperature-dependent development for arthropods. *Environmental Entomology*, 28, 22–29.

Brough, R.C., Robison, L.R. & Jackson, R.H. (1977) The historical diffusion of alfalfa. *Journal of Agronomic Education*, 6, 13–19.

Bundy, C.S., Smith, P.F., English, L.M., Sutton, D. & Hanson, S. (2005) Strain distribution of alfalfa weevil (coleoptera: curculionidae) in an intergrade zone. *Journal of Economic Entomology*, 98, 2028–2032.

Butler, G.D., Jr. & Ritchie, P.L., Jr. (1967) The life cycle of *Hypera brunneipennis* and a parasite, *Bathyplectes curculionis*, in relation to temperature. *Journal of Economic Entomology*, 60, 1239–1241.

Campbell, A., Frazer, B.D., Gilbert, N., Gutierrez, A.P. & Mackauer, M. (1974) Temperature requirements of some aphids and their parasites. *Journal of Applied Ecology*, 11, 431–438.

Cock, M.J.W., Murphy, S.T., Kairo, M.T.K., Thompson, E., Murphy, R.J. & Francis, A.W. (2016) Trends in the classical biological control of insect pests by insects: an update of the BIOCAT database. *BioControl*, 61, 349–363.

Coles, L.W. & Day, W.H. (1977) The fecundity of *Hypera postica* from three locations in the eastern United States. *Environmental Entomology*, 6, 211–212.

Cure, J.R., Rodríguez, D., Gutierrez, A.P. & Ponti, L. (2020) The coffee agroecosystem: bio-economic analysis of coffee berry borer control (*Hypothenemus hampei*). *Scientific Reports*, 10, 12262.

DeBach, P. (1964) *Biological control of insect pests and weeds*. London: Chapman and Hall.

Di Cola, G., Gilioli, G. & Baumgärtner, J. (1999) Mathematical models for age-structured population dynamics. In: Huffaker, C.B. & Gutierrez, A.P. (Eds.) *Ecological entomology*. New York, USA: Wiley.

Downie, D.A. (2010) Baubles, bangles, and biotypes: a critical review of the use and abuse of the biotype concept. *Journal of Insect Science*, 10, 176.

Du, L., Oduor, A.M.O., Zuo, W., Liu, H. & Li, J.-M. (2023) Directional and stabilizing selection shaped morphological, reproductive, and physiological traits of the invader *Solidago canadensis*. *Ecology and Evolution*, 13, e10410.

EFSA PLH Panel, EFSA Panel on Plant Health, Bragard, C., Baptista, P., Chatzivassiliou, E., Di Serio, F. et al. (2023) Assessment of the probability of introduction of *Thaumatotibia leucotreta* into the European Union with import of cut roses. *EFSA Journal*, 21(10), e08107. Available from: https://doi.org/10.2903/j.efsa.2023.8107

Gilbert, N. (1986) Control of fecundity in *Pieris rapae*. IV. Patterns of variation and their ecological consequences. *The Journal of Animal Ecology*, 55, 317.

Gilbert, N., Gutierrez, A.P., Frazer, B.D. & Jones, R.E. (1976) *Ecological relationships*. Reading and San Francisco: W.H. Freeman and Co.

Gilbert, N., Raworth, D.A. & Allen, G.R. (2010) One function of sex — an empirical study of genetic and ecological variation. *The Canadian Entomologist*, 142, 601–628.

Godefroid, M., Cruaud, A., Rossi, J.P. & Rasplus, J.Y. (2015) Assessing the risk of invasion by Tephritid fruit flies: intraspecific divergence matters. *PLoS One*, 10, e0135209.

GRASS Development Team. (2022) *Geographic resources analysis support system (GRASS) software, version 8.2.0*. Beaverton, Oregon, USA: Open Source Geospatial Foundation.

Gutierrez, A.P. (1996) *Applied population ecology: a supply-demand approach*. New York, USA: John Wiley and Sons.

Gutierrez, A.P., Christensen, J.B., Merritt, C.M., Loew, W.B., Summers, C.G. & Cothran, W.R. (1976) Alfalfa and the Egyptian alfalfa weevil (coleoptera: Curculionidae). *Canadian Entomologist*, 108, 635–648.

Gutierrez, A.P. & Ponti, L. (2013) Deconstructing the control of the spotted alfalfa aphid *Therioaphis maculata*. *Agricultural and Forest Entomology*, 15, 272–284.

Hadjistylli, M., Roderick, G.K. & Brown, J.K. (2016) Global population structure of a worldwide pest and virus vector: genetic diversity and population history of the *Bemisia tabaci* sibling species group. *PLoS One*, 11, e0165105.

Hsiao, T.H. & Hsiao, C. (1985) Hybridization and cytoplasmic incompatibility among alfalfa weevil strains. *Entomologia Experimentalis et Applicata*, 37, 155–159.

Le Roux, J. (2021) *The evolutionary ecology of invasive species*. London, UK: Academic Press.

Levi-Mourao, A., Madeira, F., Meseguer, R., García, A. & Pons, X. (2021) Effects of temperature and relative humidity on the embryonic development of *Hypera postica* Gyllenhal (Col.: Curculionidae). *Insects*, 12, 250.

Levi-Mourao, A., Madeira, F., Meseguer, R. & Pons, X. (2022) Effects of temperature on the fitness of the alfalfa weevil (*Hypera postica*). *Pest Management Science*, 78, 4223–4233.

Manetsch, T.J. (1976) Time-varying distributed delays and their use in aggregative models of large systems. In: *IEEE Transactions on Systems, Man and Cybernetics*, Vol. 6, pp. 547–553.

Marshall, K.E., Gotthard, K. & Williams, C.M. (2020) Evolutionary impacts of winter climate change on insects. *Current Opinion in Insect Science*, 41, 54–62. Available from: https://doi.org/10.1016/j.cois.2020.06.003

Messenger, P.S. & van den Bosch, R. (1969) The adaptability of introduced biological control agents. In: Huffaker, C.B. (Ed.) *Biological Control*. New York: Plenum/Rosetta Press, p. 511.

Moran, E.V. & Alexander, J.M. (2014) Evolutionary responses to global change: lessons from invasive species. *Ecology Letters*, 17, 637–649.

Morrison, W.P. & Pass, B.C. (1974) The effect of subthreshold temperatures on eggs of the alfalfa weevil. *Environmental Entomology*, 3, 353–355.

Neteler, M., Bowman, M.H., Landa, M. & Metz, M. (2012) GRASS GIS: a multi-purpose Open Source GIS. *Environmental Modelling & Software*, 31, 124–130.

Ohto, K. (1996) Effects of photoperiod on the adult diapause in the alfalfa weevil, *Hypera postica* (Gyllenhal). *Research Bulletin of the Plant Protection Service of Japan*, 32, 1–6.

Peterson, L.K. (1960) Effects of low temperature on the survival of the alfalfa weevil from Alberta and Utah. *Journal of Economic Entomology*, 53, 570–572.

Ponti, L., Gutierrez, A.P., de Campos, M.R., Desneux, N., Biondi, A. & Neteler, M. (2021) Biological invasion risk assessment of *Tuta absoluta*: mechanistic versus correlative methods. *Biological Invasions*, 23(12), 3809–3829. Available from: https://doi.org/10.1007/s10530-021-02613-5

Poos, F.W. & Bissell, T.L. (1953) The alfalfa weevil in maryland. *Journal of Economic Entomology*, 46, 178–179.

Rosenthal, S.S. & Koehler, C.S. (1968) Photoperiod in relation to diapause in *Hypera postica* from California. *Annals of the Entomological Society of America*, 61, 531–534.

Ruane, A.C., Goldberg, R. & Chryssanthacopoulos, J. (2015) Climate forcing datasets for agricultural modeling: merged products for gap-filling and historical climate series estimation. *Agricultural and Forest Meteorology*, 200, 233–248.

Saeidi, M. & Moharramipour, S. (2017) Physiology of cold hardiness, seasonal fluctuations, and cryoprotectant contents in overwintering adults of *Hypera postica* (coleoptera: Curculionidae). *Environmental Entomology*, 46, 960–966.

Salt, G. & van den Bosch, R. (1967) The defense reactions of three species of *Hypera* (coleoptera, curculionidae) to an ichneumon wasp. *Journal of Invertebrate Pathology*, 9(2), 164–177. Available from: https://doi.org/10.1016/0022-2011(67)90005-5

Sanaei, E. & Seiedy, M. (2016) Developmental differences of local populations of alfalfa weevil (*Hypera postica*) (coleoptera: Curculionidae). *Turkish Journal of Zoology*, 40, 471–479.

Sanaei, E., Seiedy, M., Skuhrovec, J., Mazur, M.A., Kajtoch, Ł. & Husemann, M. (2016) Deep divergence and evidence for translocations between Iranian and European populations of the alfalfa weevil (coleoptera: Curculionidae) based on mitochondrial DNA. *The Canadian Entomologist*, 148, 703–715.

Schroder, R.F.W. & Steinhauer, A.L. (1976) Effects of photoperiod and temperature regimens on the biology of European and United States alfalfa weevil populations. *Annals of the Entomological Society of America*, 69, 701–706.

Soroka, J.J., Bennett, A.M.R. & Mori, B.A. (2024) In: Vankosky, M.A. & Martel, V. (Eds.) *Biological Control Programmes in Canada, 2013–2023*. GB: CAB International, pp. 257–262.

Tang, F.H.M., Nguyen, T.H., Conchedda, G., Casse, L., Tubiello, F.N. & Maggi, F. (2024) CROPGRIDS: a global geo-referenced dataset of 173 crops. *Scientific Data*, 11, 413.

The MathWorks Inc. (2022) MATLAB version: 9.13.0.

Titus, E. (1910) Bulletin no. 110 – the alfalfa leaf-weevil. UAES Bulletins.

Tuda, M., Iwase, S., Kébé, K., Haran, J., Skuhrovec, J., Sanaei, E. et al. (2021) Diversification, selective sweep, and body size in the invasive

palearctic alfalfa weevil infected with *Wolbachia*. *Scientific Reports*, 11, 9664.
Van Lenteren, J.C., Bale, J., Bigler, F., Hokkanen, H.M.T. & Loomans, A.J.M. (2006) Assessing risks of releasing exotic biological control agents of arthropod pests. *Annual Review of Entomology*, 51, 609–634.
Wang, Y.H. & Gutierrez, A.P. (1980) An assessment of the use of stability analyses in population ecology. *Journal of Animal Ecology*, 49, 435–452.
Wehrle, L.P. (1940) The discovery of an alfalfa weevil (*Hypera brunneipennis* Boheman) in Arizona. *Journal of Economic Entomology*, 33, 119–121.
Zahiri, B., Fathipour, Y., Khanjani, M., Moharramipour, S. & Zalucki, M.P. (2010a) Modeling demographic response to constant temperature in *Hypera postica* (coleoptera: Curculionidae). *Journal of Economic Entomology*, 103, 292–301.
Zahiri, B., Fathipour, Y., Khanjani, M., Moharramipour, S. & Zalucki, M.P. (2010b) Preimaginal development response to constant temperatures in *Hypera postica* (coleoptera: Curculionidae): picking the best model. *Environmental Entomology*, 39, 177–189.
Zahiri, B., Fathipour, Y., Khanjani, M., Moharramipour, S. & Zalucki, M.P. (2014) Alternatives to key factor analyses for assessing the population dynamics of *Hypera postica* (coleoptera: Curculionidae). *Population Ecology*, 56, 185–194.

How to cite this article: Gutierrez, A.P., Ponti, L., Levi-Mourao, A., Pons, X., Cure, J.R., Neteler, M. et al. (2025) Stabilizing adaptation in an invasive species: Alfalfa weevil as a case study. *Agricultural and Forest Entomology*, 27(4), 573–589. Available from: https://doi.org/10.1111/afe.12686

APPENDIX: The time-invariant distributed maturation time model

The dynamics of a life stage s with $k = 1, 2,\ldots, {}^{s}k$ age classes (Equation A1, Manetsch, 1976) can be viewed as composed of ${}^{s}k$ dynamics equations. The forcing variable is temperature (T), with time (t) being a day (d) that from the perspective of poikilotherm species is of variable length in physiological time units (i.e., $0 \le {}^{s}\Delta_x(T(t))$ in degree days (dd)), or proportional development (${}^{s}r(T(t))$). Each species (and life stage) may have different mean developmental times (${}^{s}\Delta$) and temperature thresholds. The state variable ${}^{s}N_i(t)$ is the density of the i^{th} age class (mass or numbers), and ${}^{s}\mu_i(t)$ is the proportional age-specific net loss rate due to temperature, net immigration, growth in mass dynamics models, and other factors (above) during ${}^{s}\Delta_x(T(t))$ (Gutierrez, 1996). Following the notation of Di Cola et al. (1999, page 523), the i^{th} age class of stage s is modelled as follows:

$$\frac{d^{s}N_i}{dt} = \frac{{}^{s}k \cdot {}^{s}\Delta_x}{{}^{s}\Delta}\left[{}^{s}N_{i-1}(t) - {}^{s}N_i(t)\right] - {}^{s}\mu_i(t){}^{s}N_i(t). \quad \text{(A1)}$$

in terms of flux, ${}^{s}n_i(t) = {}^{s}N_i(t){}^{s}\nu_i(t)$ where ${}^{s}\nu_i(t) = \frac{{}^{s}k}{{}^{s}\Delta}\Delta_x(t)$, and

$$\frac{d}{dt}\left[\frac{{}^{s}\Delta{}^{s}n_i(t)}{{}^{s}k}\right] = {}^{s}n_{i-1}(t) - {}^{s}n_i(t) - {}^{s}\mu_i(t){}^{s}n_i(t)\frac{{}^{s}\Delta}{{}^{s}k}. \quad \text{(A2)}$$

The total density in life stage s is ${}^{s}N(t) = \sum_{i=1}^{k}{}^{s}N_i(t)$. Ignoring stage notation, new individuals enter the first age class of a stage ($i = 1$), flows occur via aging between age classes and between stages at temperature-dependent rates, with surviving adults exiting as deaths at maximum age ($i = {}^{A}k$). Absent mortality, the theoretical distribution of cohort developmental times of stage s may be estimated by Erlang parameter ${}^{s}k = {}^{s}\Delta^2/{}^{s}\sigma^2$, where σ^2 is the variance of average developmental time ${}^{s}\Delta$. Last, because of non-linearities and time-varying nature, the model can only be evaluated numerically (Wang & Gutierrez, 1980). The numerical solution for Equation A2 can be found in Abkin and Wolf (1976), and as implemented here in Gutierrez (1996, pages 157–159).